Wetting condition in diffuse interface simulations of contact line motion

Hang Ding and Peter D. M. Spelt
Department of Chemical Engineering, Imperial College London, SW7 2AZ, United Kingdom
(Received 8 January 2007; revised manuscript received 2 March 2007; published 27 April 2007)

We investigate the wetting condition for diffuse-interface methods in the simulation of two-fluid flows with moving contact lines. A current method, which uses a surface-energy approach, is shown not to result in a slope of the interface that is consistent with the prescribed value of the contact angle. A geometric formulation is proposed that does result in the prescribed contact angle. Test results are presented for the axisymmetric droplet spreading due to the capillary force and the motion of a droplet on a solid substrate in a shear flow.

DOI: 10.1103/PhysRevE.75.046708 PACS number(s): 47.11.−j, 47.55.np, 47.61.Jd

I. INTRODUCTION

Moving contact line problems are ubiquitous in nature—in everyday application and in industry—ranging from coating processes, the removal of oil from adhering surfaces in detergency applications, to water droplets rolling down leaves or window panes; wherever one fluid displaces another on a solid surface. Analysis of these problems encounters difficulties that arise from a stress singularity at a moving contact line, which results when the Navier-Stokes equations are subjected to a no-slip boundary condition at the contact line. Several explanations for the motion of contact lines have been proposed, including slip [1,2], a precursor layer [3], surface-tension relaxation [4], condensation (evaporation) [5], and a diffuse-interface formulation [6,7]. We consider the latter method in this paper.

Previous work on flows with moving contact lines predominantly uses a slip formulation, and we shall make some reference to an effective slip length in this paper, so we very briefly discuss that approach first. In that approach, the no-slip condition is replaced by a Navier slip condition, thereby introducing a "slip length" [1,2]:

$$v = \lambda \mathbf{n} \cdot \nabla \mathbf{v} \quad \text{at the wall}, \tag{1}$$

where v denotes the velocity component of fluid parallel to the solid substrate, $\mathbf{n}$ denotes the normal vector of the solid substrate, pointing into the fluid, and λ is the slip length. Amongst previous work on numerical simulations in which an approximation of the condition (1) is adopted, Schleizer and Bonnecaze [8] simulated the motion of a two-dimensional droplet in a lid-driven channel flow using the boundary element method. In our previous work, we presented a level-set approach for simulating flows with a moving contact line with hysteresis [9], and applied this method to two-dimensional droplet deformation or motion in a channel at moderate Reynolds numbers [10]. Related simulations were conducted by Zhang *et al.* [11] and Smith *et al.* [12]. In other related work, the effective slip length arising from discretization errors is exploited to allow contact lines to move [13–15].

We consider here the use of a diffuse-interface method for the simulation of these flows. This method has become very popular in recent years [7,16–21]. In this method, an order parameter (here the volume fraction of one of the fluids, denoted here by C) varies relatively smoothly in an interfacial region of finite thickness. It is known that considering a diffuse interface rather than a sharp interface around the contact line results effectively in slip, through the diffusive fluxes between the bulk fluids [22]. Hence the stress singularity at moving contact lines is removed even when a no-slip velocity boundary condition is imposed, when using a diffuse-interface method.

In order to evaluate the usefulness of this approach, and to ensure that the correct macroscopic behavior of contact line motion is obtained, there are two important issues that should be addressed. One is to relate the results to previous work, e.g., through a quantification of the effective slip length in the diffuse interface model, and the other is the appropriate formulation of the wetting condition. Jacqmin [7] and the present authors [23] have addressed the first issue in previous work. Jacqmin showed that the effective slip length λ_{di} is related to the dynamic viscosity μ and a specific parameter of the diffuse-interface model, the so-called mobility M (see Sec. II A below) by $\lambda_{di} \sim \sqrt{\mu M}$, when it is assumed that $\epsilon/\sqrt{\mu M} \to 0$, where ϵ is the characteristic length scale of diffuse interface. In previous work, we have conducted a quantitative evaluation of the effective slip length for cases where $\epsilon/\sqrt{\mu M} \sim O(1)$ through a numerical study [23], in which the numerical results of axisymmetric spreading of the droplet were compared with a lubrication theory and with results from a level-set method. The effective slip length λ_{di} was found to be approximately proportional to the characteristic length scale of the interface thinkness ϵ, i.e., $\lambda_{di} = \alpha\epsilon$, where α is a constant ($\alpha = 1.8 \pm 0.2$).

The main subject of the present paper is the second outstanding issue mentioned above, i.e., the appropriate wetting condition at the contact line for diffuse-interface methods. A so-called surface-energy formulation is generally used in the literature so far [7,16,17,19–21]. In this surface-energy formulation, the wetting condition is expressed in terms of the microscale contact angle θ_s, which can be determined by Young's equation in terms of constant surface tensions at the three material boundaries between the three phases; for example, for a gas/liquid/solid contact line,

$$\cos\theta_s = \frac{\sigma_{gs} - \sigma_{ls}}{\sigma_{lg}}, \tag{2}$$

where σ is the surface tension, and the subscripts gs, ls, and lg denote the surface tension of gas-solid, liquid-solid and

liquid-gas material boundaries, respectively. In order to establish a relationship between the microscale contact angle and the boundary condition for the order parameter, Jacqmin [7] suggested using a surface-energy density model $g(C)$ at the solid substrate. Thereby the wall surface energy is $F_w = \int \gamma g(C) dA$, where γ depends on the prescribed microscale contact angle. If the interface is in equilibrium at the solid wall, a natural boundary condition for the order parameter C can then be obtained.

$$\epsilon \mathbf{n} \cdot \nabla C = \gamma(\theta_s) g'(C) \tag{3}$$

Similar surface-energy formulations were also proposed by Papatzacos [19] and Briant *et al.* [16]. Their formulations are directly derived from Young's equation (2), in which the surface tension is computed from the excessive free energy at the interface region. The computation of liquid-gas surface tension is straightforward when the equilibrium C profile across the interface is known. However, this is not the case for the liquid-solid and gas-solid interfaces. As a result, the liquid-solid and gas-solid surface tensions are evaluated using a linear approximation of the surface-energy density model in the normal direction of the solid wall. Finally, only an approximation of the relation between γ and the microscale contact angle θ_s is provided. Papatzacos [19] showed that $\gamma = \frac{2}{3}\cos\theta_s$, and Khatavkar *et al.* [20] used $\gamma = \frac{3}{4}\cos\theta_s$. In Sec. II B below we present evidence that the application of a surface-energy formulation does not lead to a distribution of C that would be consistent with the microscale contact angle in droplet spreading. Also, a substantial difference with results from a sharp interface are observed.

In this paper we consider a droplet attached to a smooth and chemically homogeneous solid substrate such that the microcontact angle is distributed universally around the contact line. Then, we propose an alternative formulation of the wetting condition for diffuse interface simulations. This is derived strictly from the geometry of the interface in the vicinity of the contact line. We first show that the geometric formulation is equivalent to the surface-energy formulation in the computation of the contact angle when given a C distribution around a contact line. We then present evidence showing the advantages of the geometric formulation over surface-energy formulations when a contact angle is prescribed. Results from numerical validation tests are presented, including the axisymmetric droplet spreading and three-dimensional (3D) droplet displacement in a shear flow, elucidating the significance of the geometric wetting condition on the motion of the contact line.

II. MATHEMATICAL FORMULATION

A. Diffuse interface method

We consider here two incompressible immiscible fluids and assume that the density ρ and the viscosity μ is constant in each bulk fluid. The two fluids are separated by a diffuse interface that is of finite thickness, due to the mutual diffusion of the fluids. Hence the transition of physical parameters such as density, viscosity, and pressure is smooth across the interface. We define here the volume fraction C of one of the two fluids as the order parameter, such that

$$C = \begin{cases} 1 & \text{in cells occupied by fluid 1,} \\ 0 & \text{in cells occupied by fluid 2.} \end{cases} \tag{4}$$

The density and viscosity are averaged in terms of C according to

$$\rho = C\rho_1 + (1-C)\rho_2 \quad \text{and} \quad \mu = C\mu_1 + (1-C)\mu_2, \tag{5}$$

where ρ is the density, μ is the dynamic viscosity, and the subscript distinguishes the two fluids.

The scalar field of C is advected by the incompressible velocity field $\mathbf{u}$, while being diffused due to spatial inhomogeneities of the fluids. The spatiotemporal evolution of C is modeled by the convective Cahn-Hilliard (CH) equation

$$\frac{\partial C}{\partial t} + \mathbf{u} \cdot \nabla C = M \nabla^2 \phi, \tag{6}$$

where M is the mobility and ϕ is the chemical potential. When the velocity field is required to be solenoidal,

$$\nabla \cdot \mathbf{u} = 0, \tag{7}$$

the CH equation (7) conserves the total volume of each fluid, and consequently, we ensure mass conservation, even in the cases where significant density differences are involved [24].

The velocity field is the solution of the Navier-Stokes equation, given here in dimensionless form,

$$\hat{\rho}\left(\frac{\partial \mathbf{u}}{\partial t} + \mathbf{u} \cdot \nabla \mathbf{u}\right) = -\nabla p + \frac{1}{\mathrm{Re}} \nabla \cdot [\hat{\mu}(\nabla \mathbf{u} + \nabla \mathbf{u}^T)] + \frac{\mathbf{f}_{\mathbf{st}}}{\mathrm{ReCa}}, \tag{8}$$

where the dimensionless number is defined with respect to the properties of fluid 1: the Reynolds number is defined as $\mathrm{Re} = \rho_1 UL/\mu_1$, the capillary number as $\mathrm{Ca} = \mu_1 U/\sigma$, $\hat{\rho} = C + (1-C)\rho_2/\rho_1$, and $\hat{\mu} = C + (1-C)\mu_2/\mu_1$. U, L, and $\mathbf{f}_{\mathbf{st}}$ represent characteristic velocity, length, and the surface tension scales, respectively.

The profile of C across the diffuse interface is determined primarily by the free energy model, taken here as the van der Waals free energy density model in terms of volume fraction C (following, e.g., [7]),

$$f = \frac{1}{2}\epsilon\sigma\alpha|\nabla C|^2 + \epsilon^{-1}\sigma\alpha\Psi(C), \tag{9}$$

where $\Psi(C) = \frac{1}{4}C^2(1-C)^2$ is the bulk free energy density, of which two minima at $C=0$ and 1 correspond to the two bulk free energy densities, respectively; the first term on the right-hand side is the excess free energy density, and represents a measure of the local spatial inhomongeneity; σ is the coefficient of surface tension and ϵ is a measure of the interface thickness. The free energy is given by $F = \int_\Omega f\, dV$, where Ω is the physical space occupied by two fluids. The chemical potential ϕ is defined as the rate of change of free energy with respect to C,

$$\phi = \frac{\delta F}{\delta C} = \epsilon^{-1}\sigma\alpha\frac{\partial \Psi}{\partial C} - \epsilon\sigma\alpha\nabla^2 C, \tag{10}$$

where $\delta/\delta C$ denotes the variational differentiation with respect to C. When the interface is at equilibrium in the ab-

sence of fluid flow, the diffuse flux vanishes in the interfacial region. The equilibrium interface profile can then be found by solving $\phi(C)=0$. The solution for a one-dimensional profile of C at such an equilibrium is

$$C(\xi) = \frac{1}{2} + \frac{1}{2}\tanh\left(\frac{\xi}{2\sqrt{2}\epsilon}\right). \tag{11}$$

Note that though Eq. (11) is derived for a flat interface at equilibrium, it can also be used for a curved interface as long as the thickness of the diffuse interface is much smaller than the radius of the interfacial curvature.

In equilibrium the surface-tension force can be interpreted as the integral of the excess free energy per unit surface area across the interface, which yields for a flat interface

$$\sigma = \sigma\epsilon\alpha\int_{-\infty}^{+\infty}\left(\frac{dC}{d\xi}\right)^2 d\xi, \tag{12}$$

where ξ denotes the coordinate along the direction normal to the interface. The value of parameter α follows from these results as $\alpha=6\sqrt{2}$. Substituting Eq. (10) into Eq. (6) and setting $\alpha=6\sqrt{2}$, the dimensionless CH equation becomes

$$\frac{\partial C}{\partial t} + \mathbf{u}\cdot\nabla C = \frac{1}{\mathrm{Pe}}\nabla^2\left(C_h^{-1}\frac{\partial \Psi}{\partial C} - C_h\nabla^2 C\right), \tag{13}$$

where the Péclet number $\mathrm{Pe}=\frac{UL^2}{6\sqrt{2}M\sigma}$ and the Cahn number $C_h=\epsilon/L$.

The stress term in the momentum equation arising from composition gradients can be written as [25]

$$\mathbf{f_{st}} = -C\nabla\phi. \tag{14}$$

By defining $\hat{p}=p-\phi C$, this potential form of the surface-tension force can also be written as

$$\mathbf{f_{st}} = \phi\nabla C = 6\sqrt{2}\left(C_h^{-1}\frac{\partial \Psi}{\partial C} - C_h\nabla^2 C\right)\nabla C. \tag{15}$$

It is clear that the surface-tension force formulation adopted here [Eq. (15)] requires less smoothness of the chemical potential than the formulation (14). The modified pressure $\hat{p}$ aims to ensure the divergence-free velocity field constraint during the computation. For simplicity, we shall drop the caret diacritic.

We have shown previously [24] that nonpenetration of mass diffuse flow at the solid substrate is necessary for the volume conservation of each fluid in the contact line problem, i.e.,

$$\mathbf{n}\cdot\nabla\phi = 0, \tag{16}$$

where $\mathbf{n}$ is the unit outward normal defined at the solid substrate. This is one of the boundary conditions for the CH equation enforced at the solid substrate, and the other one will be derived from the wetting property of the two fluids.

B. Wetting condition

As discussed in the Introduction, boundary conditions for the CH equation based on a surface-energy formulation are currently popular in diffuse-interface methods for moving-contact-line problems. In this section, we briefly derive this condition, together with an alternative, using the geometrical properties of the order parameter C at the contact line. Both boundary conditions are tested in Sec. IV below.

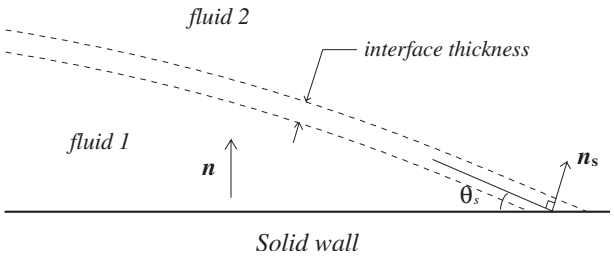

FIG. 1. Diffuse interface interpretation of the contact line and the contact angle

If the contours of the order parameter in the diffuse interface are approximately parallel to each other, the normal vector to the interface (denoted by $\mathbf{n_s}$) can be written in terms of the gradient of C as

$$\mathbf{n_s} = \nabla C/|\nabla C|. \tag{17}$$

At the contact line, $\mathbf{n_s}$ intersects the solid substrate at an angle of $\pi/2-\theta$, where θ is the contact angle (see Fig. 1). Thus, the contact angle can be computed geometrically in terms of C by

$$\tan\left(\frac{\pi}{2}-\theta\right) = \frac{-\mathbf{n}\cdot\nabla C}{|\nabla C - (\mathbf{n}\cdot\nabla C)\mathbf{n}|}. \tag{18}$$

Equation (18) is herein referred to as a *geometric formulation* for the computation of the contact angle θ. This formulation provides a good approximation of the contact angle θ as long as (a) there are enough grid points (usually 4–8) to resolve the interface, and (b) the diffuse interface is in equilibrium or near equilibrium at the solid substrate; in other words, as long as the interface in the neighborhood of the contact line is not significantly thinned or thickened during the computation.

Equation (18) can also be written as

$$\mathbf{n}\cdot\nabla C = -|\nabla C|\cos\theta. \tag{19}$$

Multiplying both sides of Eq. (17) with $\mathbf{n_s}$ results in

$$|\nabla C| = \mathbf{n_s}\cdot\nabla C = \partial C/\partial n_s. \tag{20}$$

Upon substituting the equilibrium interfacial profile Eq. (11), Eq. (20) becomes, after some manipulations,

$$|\nabla C| = \frac{C(1-C)}{\sqrt{2}\epsilon} = \frac{\sqrt{2\Psi(C)}}{\epsilon}. \tag{21}$$

Substitution of Eq. (21) into Eq. (19) gives

$$\cos\theta = -\frac{\epsilon\mathbf{n}\cdot\nabla C}{\sqrt{2\Psi(C)}}, \tag{22}$$

which is herein referred to as a *surface-energy formulation* for the computation of the microscale contact angle θ. We conclude that the geometric formulation (18) and surface-

energy formulation (22) are equivalent in computing the contact angle θ for a given C distribution in the immediate vicinity of a contact line.

The formulations for computing the microscale contact angle can also be converted into wetting conditions for a prescribed microscale contact angle θ_s. For example, the wetting condition of surface-energy form can be straightforwardly obtained from Eq. (22).

$$\epsilon \mathbf{n} \cdot \nabla C = -\sqrt{2} \cos \theta_s \sqrt{\Psi(C)}. \tag{23}$$

It is easy to show that Eq. (23) is of the same form as the wetting condition used in [20], by using the same order parameter as in that paper. The sole difference between the two results, is in fact, that the current approach gives

$$\gamma = \frac{1}{\sqrt{2}} \cos \theta_s, \tag{24}$$

whereas the value of the constant coefficient on the right-hand side obtained by Papatzacos [19] is 0.67, and 0.75 by Khatavkar *et al.* [20]. Our result for the surface-energy formulation, which indeed involves a geometrical argument, is just in-between these results that involved an approximation at some point. The corresponding wetting condition for the geometric formulation is

$$\mathbf{n} \cdot \nabla C = -\tan\left(\frac{\pi}{2} - \theta_s\right) |\nabla C - (\mathbf{n} \cdot \nabla C)\mathbf{n}|. \tag{25}$$

We now investigate whether the two wetting conditions are also equivalent when a microscale contact angle θ_s is prescribed. In order to compare Eq. (25) with the surface-energy formulation, we write the latter in the form given in Eq. (19),

$$\mathbf{n} \cdot \nabla C = -|\nabla C| \cos \theta_s. \tag{26}$$

In order to assess whether the boundary conditions (24)–(26) ensure that the correct microscale contact angle will be imposed, we consider here the case wherein for some kind of numerical reason initially the value of the contact angle (denoted here by θ_d) may be different from the prescribed microscale contact angle θ_s. This is in fact what happens in the simulations presented in this paper: at each time step, C is first updated in the volume occupied by both fluids, while the values at ghost cells are fixed; the latter are updated subsequently such as to represent the boundary condition imposed.

It is important to note that in numerical simulations the wetting condition should ensure that the contact angle θ is equal to the microscale contact angle θ_s at each time step only by adjustment of $\mathbf{n} \cdot \nabla C$ (e.g., at ghost cells in the wall). The reason for this is that the magnitude of the tangential component of ∇C ($=\mathbf{t} \cdot \nabla C$, where $\mathbf{t}$ denotes the direction parallel to the solid substrate, in the plane defined by $\mathbf{n}$ and $\mathbf{n_s}$) cannot be changed. It is therefore essential to express the right-hand sides of Eqs. (25) and (26) in terms of $\mathbf{t} \cdot \nabla C$. The wetting condition following from the present geometrical arguments (25) leads to the following boundary condition for C:

$$\mathbf{n} \cdot \nabla C = -\cos \theta_s |\mathbf{t} \cdot \nabla C| / \sin \theta_s, \tag{27}$$

while the surface-energy formulation of the wetting condition results in

$$\mathbf{n} \cdot \nabla C = -\cos \theta_s |\mathbf{t} \cdot \nabla C| / \sin \theta_d \tag{28}$$

by substituting $|\nabla C| = \mathbf{t} \cdot \nabla C / \sin \theta_d$ into Eq. (26). We can see that the microscale contact angle can be reproduced from the local distribution of C after the implementation of Eq. (27). However, this is not the case when using Eq. (28). In fact, the boundary condition (28) is comparable to imposing an effective contact angle θ, where $\min(\theta_s, \theta_d) \leq \theta \leq \max(\theta_s, \theta_d)$, instead of the microscale contact angle. Tracing back the difference between the two conditions, the cause is seen to be the fact that in Eq. (25) only the tangential component of ∇C appears on the right-hand side, whereas all components of ∇C are present on the right-hand side of Eq. (26). The application of either boundary condition will in fact change the normal component $\mathbf{n} \cdot \nabla C$, which will therefore affect the right-hand side of the latter, but not the former.

Hence the use of the surface energy in the numerical simulations with moving contact lines is expected to lead to values of the contact angle that differ from the prescribed value with the exception of $\theta_s = \pi/2$, for which both the geometric and surface-energy formulation yield $\mathbf{n} \cdot \nabla C = 0$. We conclude therefore that it is safer and more efficient to use the geometric formulation in practical applications. Qian *et al.* [26] also noticed the difference between the effective contact angle θ and the microscale contact angle θ_s arising from the surface-energy formulation. They made an effort to improve the surface-energy formulation by introducing the concept of *compensated Young stress*, which allows a relaxation of the resulting dynamic contact angle and thereby makes it closer to the microscale contact angle than the effective contact angle. Their relaxation scheme alleviates the deviation of the resulting contact angle from the microscale contact angle; however, it does not completely resolve it.

III. NUMERICAL METHODS

Numerical discretization is carried out on a staggered grid with a grid size of $h = \Delta x = \Delta y$. On the staggered grid, the scalar flow variables such as pressure and volume fraction are defined at the center of each cell, and the velocity components at the corresponding cell faces. The Adams-Bashforth scheme and Crank-Nicolson schemes are employed in the discretization of the Navier-Stokes (NS) and CH equations, which involves three time steps: $n-1$, n, and $n+1$. All the dependent variables everywhere in the domain are supposed to be known only at time steps $n-1$ and n. To advance the dependent variables to time step $n+1$, three (sub-)steps are performed:

(a) Update the volume fraction field by solving the CH Eq. (6) with the velocity and C field at time steps $n-1$ and n;

(b) Compute the local surface-tension force in the interfacial region at time step $n+1/2$ using the volume fraction field at time steps n and $n+1$;

(c) Update the velocity field to time step $n+1$ by solving the NS Eqs. (7) and (8). Details of the solutions of CH and

NS equations can be found in [24]. Here, we mainly focus on the implementation of the geometric formulation of the wetting condition.

The wetting condition provides a natural boundary condition for the solution of the CH equation. Since the volume fraction C is defined at cell centers, one layer of ghost cells is used to enforce the boundary conditions. Hence the implementation of the wetting condition corresponds to the determination of the value of C at the center of the ghost cells. In the following, we shall explore the details of how to impose the two wetting conditions on a staggered grid. We consider here the cell centers $(i,1)$ adjacent to the solid substrate, where the first index i denotes the coordinate tangential to the solid substrate and the second index denotes the coordinate normal to the solid substrate. If $0.001 < C_{i,1} < 0.999$, the cell centers $(i,1)$ are considered to be located in the contact line region. Applying a central finite difference scheme to discretize the derivatives on both sides of the wetting condition (27) at the cell center $(i,1)$, we can obtain an approximation of $C_{i,0}$ from the C values at its neighboring cell centers,

$$C_{i,0} = C_{i,2} + \tan\left(\frac{\pi}{2} - \theta_s\right)|C_{i+1,1} - C_{i-1,1}|. \tag{29}$$

This equation serves as the discretized wetting condition for a prescribed microscale contact angle θ_s. Note that all C values on the right-hand side of Eq. (29) are supposed to have already been updated to time step $n+1$, and can therefore be used to extrapolate $C_{i,0}^{n+1}$.

The no-penetration of the diffuse flux provides a further boundary condition for the CH equation, i.e., Eq. (16). It is used to determine the chemical potential at the ghost-cell center $(i,0)$ by $\phi(i,0) = \phi(i,1)$. This condition is very helpful in keeping the total mass conserved [24].

IV. RESULTS AND DISCUSSION

A. Capillary spreading

The first test case considered here is the axisymmetric spreading of a droplet on a solid substrate, in which a capillary force drives the flow and the motion of the contact line. This flow is analyzed in detail in Ref. [23]; we focus here on the implementation of the wetting condition. The features of the dynamical behavior of droplet spreading are observed on a inertial-capillary time scale $T = \sqrt{\rho a_0^3/\sigma}$ [27], where a_0 is the initial radius of the droplet. The results are presented for fixed values of the Ohnesorge number

$$\mathrm{Oh} = \sqrt{\mathrm{Ca/Re}} = \frac{\mu}{\sqrt{\rho\sigma a_0}}. \tag{30}$$

In the following simulations, we use a grid of 401×161 for a domain of 2×0.8, and set $\mathrm{Oh} = 0.0354$ and the Cahn number $C_h = \epsilon/a_0 = 0.005$, which results in an effective slip length of about $0.01a_0$. The simulation starts from an initial contact angle of $\pi/3$ and the microscale contact angle is set to $\pi/18$.

The spreading process at the initial stage can be observed in Fig. 2, where sequences of drop shapes are shown in terms of the volume fraction countour $C = 0.5$. In particular, the drop shape at $t = 0.226$ using the geometric formulation is shown in Fig. 3 in terms of the volume fraction counters ranging from $C = 0.1$ to 0.9. Because either the straining fluid flow or the wetting condition could possibly thin or thicken the interface near the contact line, it is a concern whether the volume fraction profile near the contact line is well maintained at its equilibrium state. In the present simulations we use a semiimplicit method for the convective Cahn-Hilliard equation and the wetting condition is enforced in an iterative way. Thus, these thinning (thickening) effects will be deliberately balanced by the diffusive flux at each time step to keep the profile of the interface near the contact line at equilibrium, even for moving contact lines. In Fig. 3 we can see that at that moment the interfacial profiles around the contact line are indeed at equilibrium or very close to their equilibrium state.

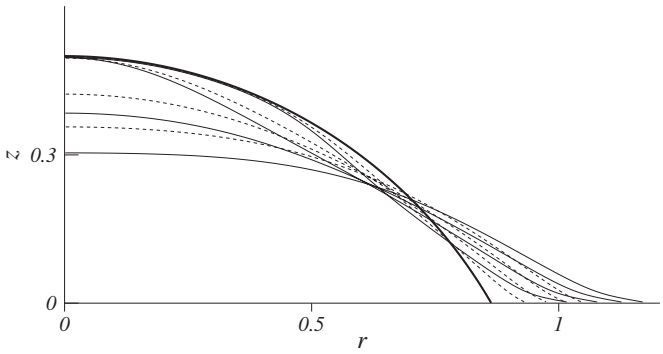

FIG. 2. Snapshots of droplet interface shapes at times $t = 0$, 0.113, 0.226, 0.452, 0.679. The thick solid line represents the initial droplet interface ($t = 0$), the solid lines are from the geometric formulation, and the dashed lines are from the surface-energy formulation.

Several observations can be made from the results of the geometric formulation and surface-energy formulation. First, the surface-energy formulation results, at any given time, in a larger value of the dynamic contact angle than the geometric formulation (see Fig. 2). Figure 4 shows the difference between the microcontact angle and the effective contact angle obtained by the surface-energy formulation, as a function of time in a semilogarithmic plot. It is seen that the effective contact angle gradually relaxes to the microscale

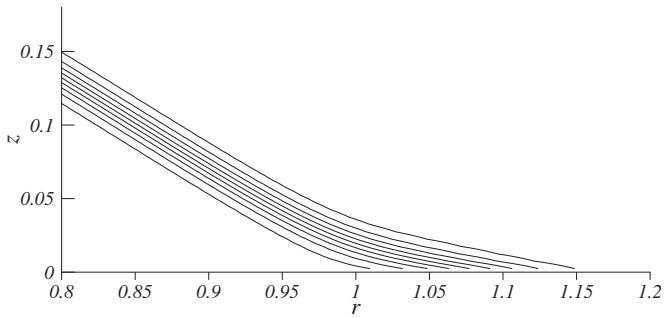

FIG. 3. Drop shape around the contact line at time $t = 0.226$ in terms of contours ranging from $C = 0.1$ to 0.9. The results are obtained using the geometric formulation.

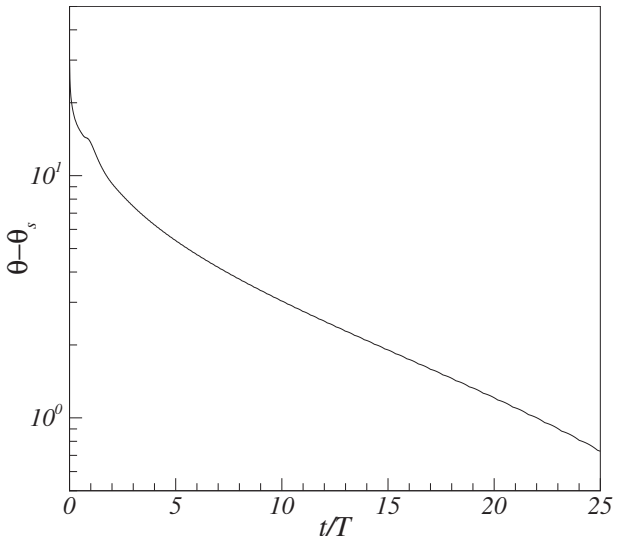

FIG. 4. Difference between the contact microscale contact angle and the effective contact angle obtained using surface-energy formulation as a function of time.

contact angle. Inertial effects account for the nonmonotoneous relaxation of the effective contact angle at the early stage of spreading [23]. At the late stage the effective contact angle converges exponentially to the microcontact angle. Secondly, it is found that the spreading process using the surface-energy formulation is relatively slower than when the geometric formulation is used. These two observations agree with our analysis in Sec. II B, i.e., surface-energy formulation generally enforces an intermediate contact angle value $\theta[\min(\theta_s,\theta_d)\leq\theta\leq\max(\theta_s,\theta_d)]$. It is due to this fact that the spreading process is considerably delayed when using the surface-energy formulation.

For comparison we have also obtained results from a level-set method simulation [9], which uses a slip condition (1). We reproduce from [23] a comparison in Fig. 5 between results obtained from a level-set method (for a fitted slip length of $0.01a_0$) and the current diffuse-interface method. Here the maximum angle between the interface and the horizontal in a small region around the contact line (indicative of an apparent contact angle) is plotted as a function of the instantaneous capillary number $\mathrm{Ca}_{cl}=\mu U_{cl}/\sigma$. The results obtained by the level-set method agree very well with those of the diffuse-interface method using the geometric formulation for this fitted "effective" slip length for $\mathrm{Ca}_{cl}\leq 0.02$. A possible explanation for the differences at larger values of Ca_{cl} is that at that stage of the simulations (i.e., directly after $t=0$), the radius of curvature is too small to expect good agreement between the two methods. It is seen that the surface-energy formulation leads to a solution that is substantially different from the level-set method at this slip length (it is only in the limit of $\mathrm{Ca}_{cl}\to 0$, i.e., the steady state of the droplet, that all the results appear to converge). Given the strong time dependence of the contact angle in this simulation (cf. Fig. 4), which evidently affects the results in Fig. 5, we have not attempted to conduct a simulation using a level-set simulation with a fitted slip-length (also, the slip length value required would be excessively small).

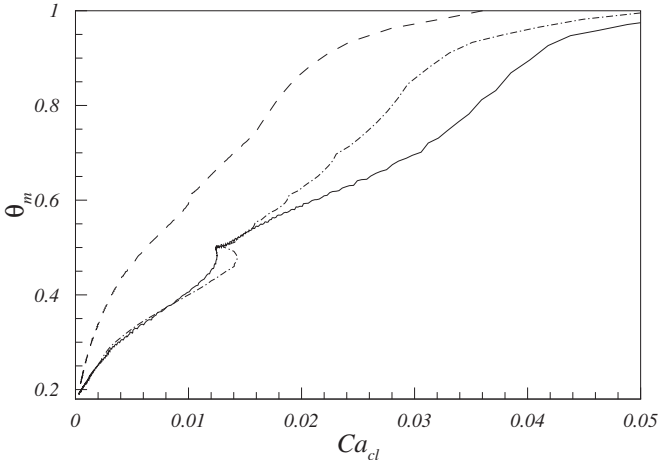

FIG. 5. Maximum apparent contact angle as a function of the capillary number. The dashed-dotted, dashed, and solid lines indicate the results from the level-set method, the surface-energy formulation, and the geometric formulation of the diffuse-interface method, respectively. Dashed-dotted and solid lines are from Ref. [23].

B. Sliding motion of a drop in shear flows

In this section we present a study of the effects of wetting conditions on fully 3D flows by simulating the sliding motion of a drop in shear flow in a channel. The microscale contact angle is prescribed as $\theta_s=\pi/3$. The computational domain is of size $15H_d\times 9H_d\times 3H_d$, where H_d is the initial height of the drop. Initially, the radius of the contact line of the drop is $\sqrt{3}H_d$, and the drop rests at $x=4.5H_d$. The upper boundary of the channel moves at a constant velocity, to produce a shear flow of shear rate $\dot{\gamma}=1/3$ in the channel. The droplet-to-outer-fluid density and viscosity ratios are $\rho_1/\rho_2=10$ and $\mu_1/\mu_2=10$, respectively. We use H_d as the charac-

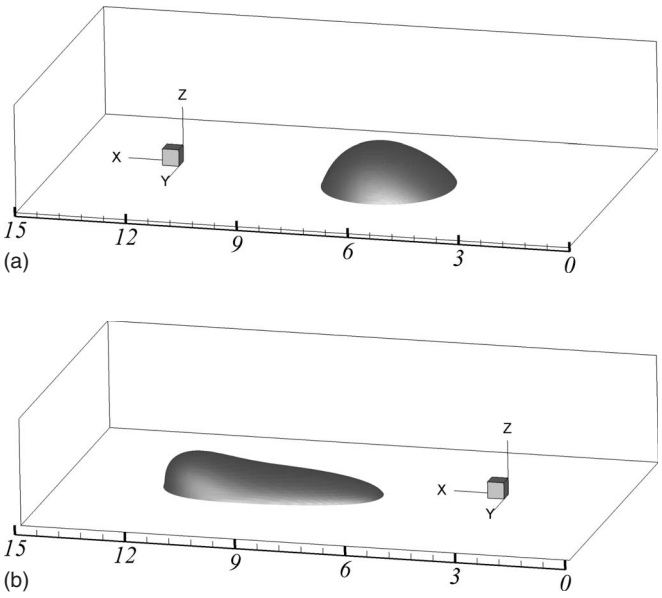

FIG. 6. Three-dimensional views of the moving drop for $\theta_s=60$, Re=8.89 and using the geometric wetting condition. (a) Ca=0.5, (b) 2.5.

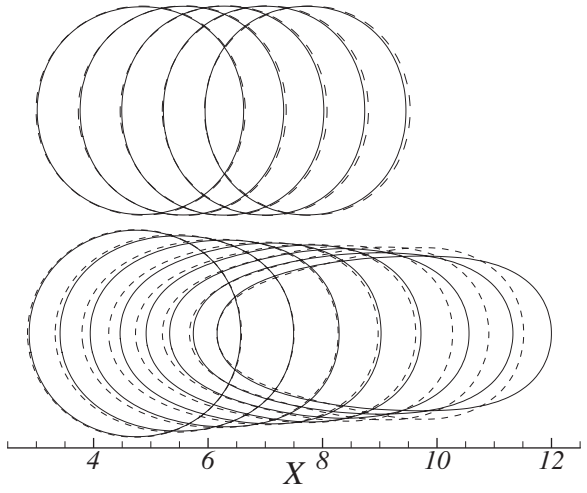

FIG. 7. Snapshots of contact lines of the moving drop (from left to right) for $\theta_s = 60°$, Re=8.89 at a time interval of 30: Ca=0.5 (upper figure), Ca=2.5 (lower figure). The solid and dashed lines represent the results when using the geometric and the surface-energy formulations of the wetting condition, respectively.

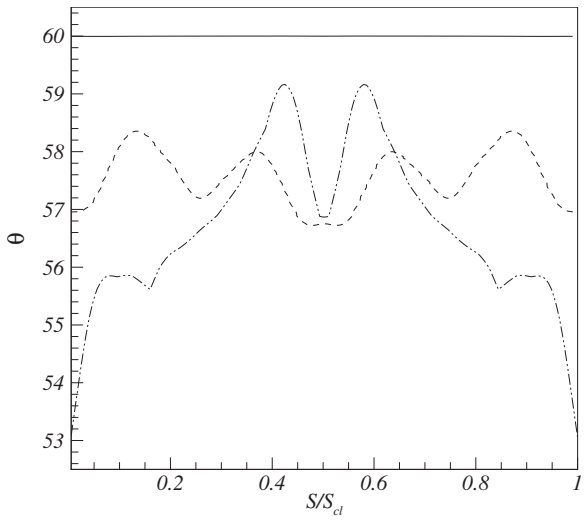

FIG. 8. Contact-angle distribution along the contact line for θ_s =60°, Re=8.89. S denotes the coordinate along the contact line starting at the upstream and S_{cl} denotes the circumference of the contact line. The solid line represents the results using the geometric formulation surface-energy formulation. The dashed and dash-dot-dotted lines represent the results using the surface-energy formulation at Ca=0.5 and 2.5, respectively.

teristic length and the inverse of the shear rate $1/\dot{\gamma}$ as the characteristic time. A Reynolds and capillary number is defined as $\mathrm{Re}=\rho_1\dot{\gamma}H_d^2/\mu_1$ and $\mathrm{Ca}=\mu_1\dot{\gamma}H_d/\sigma$, respectively. The simulations are carried out on a grid of $251\times151\times51$ with a grid size $h=0.06H_d$. In all cases, the Cahn number is set to $C_h=\epsilon/H_d=0.03$, which yields an estimated slip length of about $0.054H_d\sim0.06H_d$ [23]. The Reynolds number Re =8.89 and the initial contact angle is set to $\pi/3$, which equals the microscale contact angle.

Two test cases of respective capillary numbers Ca=0.5 and 2.5 have been investigated. The 3D views of the moving droplet using the geometric formulation are shown in Fig. 6. Generally, the differences in the motion of the contact line using geometric and surface-energy formulation are relatively modest in the test case of the small capillary number, where the surface tension is the dominant force. Snapshots of contact lines in dimensionless time intervals of 30 are shown in Fig. 7. We see that the results from the two wetting conditions generally appear to agree well at Ca=0.5; only subtle differences in the shape of contact lines are observed around the front and rear of the contact line. Comparatively significant differences occur in the test case of Ca=2.5 and they become more pronounced as the droplet undergoes considerable continuous deformation. The reason for this difference lies primarily in the effective contact angle implemented in the surface-energy formulation. The contact-angle distribution along the contact line is shown in Fig. 8, where s denotes the coordinate along the contact line and S_{cl} denotes the circumference of the contact line. It shows that the contact angle resulting from calculations wherein the geometric formulation is used always remains at the prescribed microscale contact angle, i.e., $\theta=\pi/3$, whereas the surface-energy formulation results in a deviation of the contact angle from the prescribed value. The magnitude of the deviation appears to be dependent on the capillary number, e.g., $2°-3°$ at Ca =0.5 and $1°-7°$ at Ca=2.5. The distribution of the effective contact angle arising from the surface-energy formulation does not vary monotonously from the rear to the front of the contact line. The contact-line speed is also affected by the formulation of the wetting condition. After the acceleration at the initial stage, the contact-line speed at the front and rear of the contact line gradually converges to a constant value; hence the contact-line motion reaches a steady state. At steady state, the contact-line speed U_{cl} at Ca=0.5 is approximately 0.0240 when using the geometric formulation, and 0.0242 when using the surface-energy formulation. They are very close as the resulting hysteresis is almost zero (see Fig. 8). At Ca=2.5 the contact-line speed U_{cl} is approximately 0.021 when using the geometric formulation, and 0.019 when using the surface-energy formulation. The motion of the droplet of the latter is therefore slightly hampered in the latter case, giving the appearance of contact-angle hysteresis. The effective contact angle cannot be interpreted as a dynamic contact angle, however. This is due to the fact that we do not assume any constitutive relation between the contact angle and the speed of the contact line in the present simulations, which would account for the roughness or the chemical inhomogeneity of the solid substrate. Overall, therefore, the results using the geometric formulation are expected to be superior over those from the surface-energy approach.

V. CONCLUSION

In this paper we propose a geometric formulation of wetting conditions with respect to the microscale contact angle, which can be used in the diffuse interface simulation of moving contact line problems. Compared with the widely used surface-energy formulation, we show theoretically that the geometric formulation can successfully enforce a wetting condition for a constant microscale contact angle that corre-

sponds to a smooth and chemically homogeneous solid surface, while the surface-energy formulation actually would result in a deviated value. This analysis is supported by the numerical experiments such as the capillary spreading and the 3D moving droplet under shear flows. In summary, both the theoretical analysis and numerical results for capillary spreading indicate that the geometric formulation is technically more feasible than the surface-energy formulation in diffuse-interface simulations.

ACKNOWLEDGMENTS

We wish to acknowledge financial support from EPSRC under Grant No. EP/D031222.

[1] C. Huh and L. E. Scriven, J. Colloid Interface Sci. **35**, 85 (1971).
[2] L. M. Hocking, J. Colloid Interface Sci. **76**, 801 (1976).
[3] P. G. de Gennes, Rev. Mod. Phys. **57**, 827 (1985).
[4] Y. D. Shikhmurzaev, J. Fluid Mech. **334**, 211 (1997).
[5] Y. Pomeau, C. R. Acad. Sci. Paris, Ser. IIb **328**, 411 (2000).
[6] P. Seppecher, Int. J. Eng. Sci. **34**, 977 (1996).
[7] D. Jacqmin, J. Fluid Mech. **402**, 57 (2000).
[8] A. D. Schleizer and R. T. Bonnecaze, J. Fluid Mech. **383**, 29 (1999).
[9] P. D. M. Spelt, J. Comput. Phys. **207**, 389 (2005).
[10] P. D. M. Spelt, J. Fluid Mech. **561**, 439 (2006).
[11] J. Zhang, M. J. Miksis, and S. G. Bankoff, Phys. Fluids **18**, 072106 (2006).
[12] K. A. Smith, J. M. Ottino, and P. B. Warren, Ind. Eng. Chem. Res. **44**, 1194 (2005).
[13] J. A. Moriarty and L. W. Schwartz, J. Eng. Math. **26**, 81 (1992).
[14] M. Renardy, Y. Renardy, and J. Li, J. Comput. Phys. **171**, 243 (2001).
[15] A. Mazouchi, C. M. Gramlich, and G. M. Homsy, Phys. Fluids **16**, 1647 (2004).
[16] A. J. Briant, A. J. Wagner, and J. M. Yeomans, Phys. Rev. E **69**, 031602 (2004).
[17] A. J. Briant and J. M. Yeomans, Phys. Rev. E **69**, 031603 (2004).
[18] P. Yue, J. J. Feng, C. Liu, and J. Shen, J. Fluid Mech. **515**, 293 (2004).
[19] P. Papatzacos, Transp. Porous Media **49**, 139 (2002).
[20] V. V. Khatavkar, P. D. Anderson, and H. E. H. Meijer, J. Fluid Mech. **572**, 367 (2007).
[21] W. Villanueva and G. Amberg, Int. J. Multiphase Flow **32**, 1072 (2006).
[22] H. Y. Chen and D. Jasnow, Phys. Rev. Lett. **85**, 1686 (2000).
[23] H. Ding and P. D. M Spelt, J. Fluid Mech. **576**, 287 (2007).
[24] H. Ding, P. D. M. Spelt, and C. Shu, J. Comput. Phys. (to be published).
[25] D. Jacqmin, J. Comput. Phys. **155**, 96 (1999).
[26] T. Z. Qian, X. P. Wang, and P. Sheng, J. Fluid Mech. **564**, 333 (2006).
[27] A.-L. Biance, C. Clanet, and D. Queré, Phys. Rev. E **69**, 016301 (2004).